

Fluctuation-induced dynamo effect in a magnetic confinement plasma

W. Z. Mao¹, W. X. Ding^{1,2,*}, H. Q. Liu^{3,†}, A. Ti³, D. L. Brower², H. Lian², Y. Q. Chu², L. Zeng³, H. L. Zhao³, L. Zhang³, J. P. Qian³, Q. Zang³, X. Z. Gong³, L. Q. Hu³, L. Q. Xu³, C. Zhou¹, T. Lan¹, A. D. Liu¹, J. L. Xie¹, G. Zhuang¹, Y. T. Song³, B. N. Wan^{1,3} and J. G. Li^{1,3}

¹*School of Nuclear Science and Technology, University of Science and Technology of China, Hefei 230026, People's Republic of China*

²*University of California Los Angeles, Los Angeles, California 90095, USA*

³*Institute of Plasma Physics, Chinese Academy of Sciences, Hefei 230031, People's Republic of China*



(Received 7 December 2022; accepted 12 May 2023; published 5 June 2023; corrected 9 November 2023)

The electron temperature fluctuation-induced dynamo electric field has been measured in the core of high-temperature EAST tokamak plasmas by Faraday-effect polarimetry and electron cyclotron emission. It is found that a dynamo electric field primarily arises from the coherent interaction between radial magnetic-field fluctuations and electron temperature fluctuations associated with the internal kink instability, acting to self-regulate the current profile to prevent sawtooth magnetic reconnection.

DOI: [10.1103/PhysRevResearch.5.L022047](https://doi.org/10.1103/PhysRevResearch.5.L022047)

Dynamo effect, or transport of field-aligned current whereby a self-generated electric current or magnetic field [1,2] can arise from a fluctuation-induced electromotive mean field (emf), is an important physical phenomena in both astrophysical [3] (e.g., solar coronal loops [4], galactic formation [5,6]) and laboratory plasmas [7,8]. In recent years, the magnetohydrodynamic (MHD) and Hall dynamos have been experimentally measured in reversed-field pinch plasmas [9–14] and are considered the dominant mechanism for magnetic-field generation and anomalous current transport. Sawtooth crash is a ubiquitous phenomenon in tokamak plasmas during which the core current falls suddenly due to magnetic reconnection. The sawtooth crash affects energy confinement and can trigger the neoclassical tearing mode, leading to discharge termination (disruption), hence requiring it to be suppressed to achieve the safe operation of a tokamak reactor [15–17]. It is generally thought that a helical internal $[(m, n) = (1, 1)$, where m and n are poloidal and toroidal mode numbers, respectively] kink/tearing instability plays an important role in sawtooth events, where a magnetic reconnection process occurs on resonant surfaces with rational values of the safety factor $q = 1$ (here, $q = d\psi_t/d\psi_p$, and ψ_t and ψ_p are the toroidal and poloidal magnetic fluxes, respectively). As a consequence of reconnection, current density (poloidal flux) drops (q at the magnetic axis increases) and thermal energy redistributes. However, it has been long observed in the magnetic confinement plasmas that the (1,1) mode can persist much longer than the energy confinement time with-

out reconnection (or pressure flattening) occurring, where the safety factor profile remains flat and clamped near unity [18,19], suggesting there exists an unknown current transport mechanism acting to prevent current profile peaking.

Dynamo effects have been investigated in tokamak plasmas both theoretically [20,21] and experimentally [8,22–25]. Direct measurements of magnetic flux pumping (current transport) confirm there is a dynamo effect in tokamak plasmas where MHD activity is thought to be critical [22]. However, identifying the origin of dynamo electric field in tokamak plasmas remains extremely challenging since it demands simultaneous measurements of magnetic and flow fluctuations. Recently, Jardin *et al.* [26] proposed a new theory for sawtooth-free operation in inductively driven discharges, where a dynamo voltage can be produced by a nonlinearly saturated (1,1) interchange mode. Theoretically, a $\vec{E} \times \vec{B}$ flow-driven dynamo effect is proposed to explain the “hybrid” mode [27,28], where the flow is a self-organized effect attributed to MHD modes, such as internal saturated modes in a steady-state, nonaxisymmetric, magnetic equilibrium or nonlinearly coupled tearing modes [22]. In addition, it is shown in global gyrokinetic simulations that small-scale turbulence can also generate a plasma current in different plasma regions [29].

Parallel current transport driven by instabilities is described by parallel Ohm's law [30], where all applied forces are balanced by frictional drag [31] according to

$$-\frac{m_e}{e^2 n_e} \frac{\partial \vec{J}}{\partial t} + \vec{E} + \vec{v}_e \times \vec{B} + \frac{\nabla P_e}{en_e} = \eta \vec{J}, \quad (1)$$

where n_e is electron density, e is electron charge, \vec{J} is plasma current density, P_e is the electron pressure, \vec{E} is the electric field, and electron velocity is $\vec{v}_e = \vec{v}_i - \vec{J}/ne$, where \vec{v}_i is ion velocity or plasma velocity. \vec{B} is magnetic field and η is the electric resistivity. By decomposing each quantity into mean and fluctuating parts, and taking the ensemble average of the

*Corresponding author: wding@ucla.edu

†Corresponding author: hqliu@ipp.ac.cn

parallel component over a flux surface [14], we find

$$\eta_{\parallel} \langle \vec{J} \rangle_{\parallel} - \langle \vec{E} \rangle_{\parallel} = \langle \delta \vec{v}_e \times \delta \vec{B} \rangle_{\parallel}, \quad (2)$$

where δ implies a fluctuation quantity, and $\langle \dots \rangle$ denotes flux surface averaging. The perpendicular components of $\delta \vec{v}_e$ can result from electric field and pressure fluctuations. Therefore, parallel Ohm's law can be rewritten as

$$\eta_{\parallel} \langle \vec{J} \rangle_{\parallel} - \langle \vec{E} \rangle_{\parallel} = \langle \delta \vec{E}_{\perp} \cdot \delta \vec{b}_{\perp} \rangle + \frac{\langle \nabla_{\perp} \delta P_e \cdot \delta \vec{b}_{\perp} \rangle}{en_e}, \quad (3)$$

where $\vec{b} = \vec{B}/B$ is the unit magnetic field and \vec{b}_{\perp} is its perpendicular component. The right-hand side (rhs) of Eq. (3) consists of two terms: the first term arising from the correlation of electric and magnetic fluctuations associated with the electrostatic $\vec{E} \times \vec{B}$ flow, and the second term arising from the correlation of electron pressure gradient and magnetic fluctuations related to diamagnetic flow fluctuations. The first term is a single fluid effect commonly referred to as the MHD dynamo, and the second term is an electron fluid effect called the diamagnetic dynamo [14]. Furthermore, electron pressure fluctuations arise from density fluctuation (δn_e) and temperature fluctuation (δT_e), i.e. $\delta P_e = T_e \delta n_e + n_e \delta T_e$. Hence, we can rewrite the diamagnetic dynamo term, in cylindrical coordinates, as [32]

$$\frac{\langle \nabla_{\perp} \delta P_e \cdot \delta \vec{b}_{\perp} \rangle}{en_e} \approx \frac{\langle T_e \rangle}{e \langle n_e \rangle B} \left\langle \frac{\partial \delta n_e}{\partial r} \delta b_r \right\rangle + \frac{1}{eB} \left\langle \frac{\partial \delta T_e}{\partial r} \delta b_r \right\rangle, \quad (4)$$

where the first term on the rhs is the δn_e -driven dynamo emf, and the second term is the δT_e -driven dynamo emf, and δb_r are the radial magnetic fluctuations. In order to investigate dynamo effects induced by fluctuations in parallel-current transport, one has to measure the correlated product of two fluctuating quantities. In general, the total current density could also be impacted by other dynamo actions, such as the dynamo arising from electrostatic fluctuations (e.g., interchange mode) in Eq. (3). A basic understanding of fluctuation-induced dynamo processes is of great interest as it involves self-organization behavior in which fluctuations are both destabilized by, and contribute to, the shape of the equilibrium profiles. In addition, the dynamo effect is potentially critical to current profile control and plasma stability for future burning plasmas like ITER. To date, direct measurements of diamagnetic dynamos could only be made in the lower temperature plasma edge using probes [14].

In this Letter, we present the first measurement of the diamagnetic dynamo resulting from the correlated product of magnetic and electron temperature fluctuations in high-temperature, collisionless EAST tokamak plasmas. The fluctuation-induced dynamo is found to be significant and redistributes the field-aligned current, preventing sawtooth reconnection events, thereby suggesting that steady-state, sawtooth-free discharges can be sustained by continuous current relaxation in plasmas.

Measurement of the fluctuation-induced dynamo associated with the internal (1,1) MHD instability has been achieved on high-temperature EAST plasmas. EAST (major radius, $R \leq 1.9$ m; minor radius, $a \leq 0.45$ m) is a fully superconducting tokamak with an ITER-like tungsten divertor. A previously reported discharge [33] is shown in Fig. 1 (shot 70187)

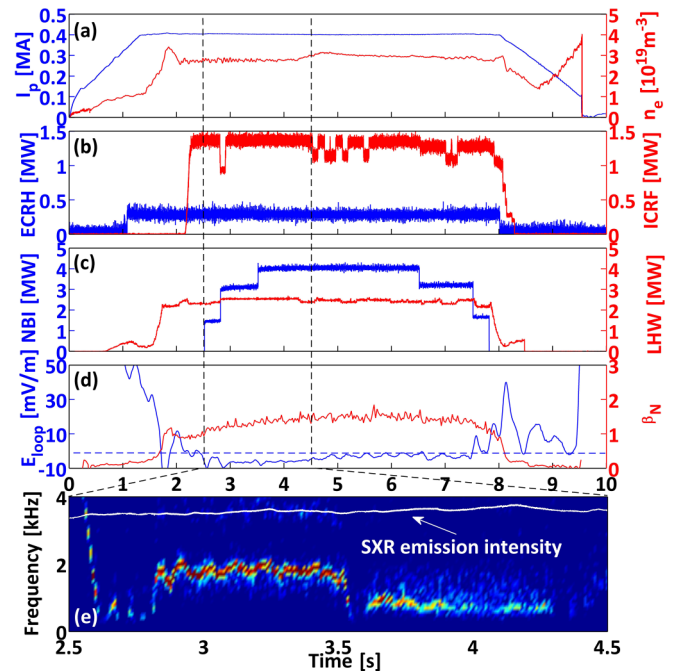


FIG. 1. (a) Discharge current and the line-averaged density; (b) ECRH and ICRF wave power; (c) NBI and LHW power; (d) external loop emf and normalized plasma pressure β_N , where the horizontal dashed black line in (d) indicates zero surface electric field; and (e) soft x-ray (SXR) emission spectra for viewing the passing plasma center. Emission intensity (white) shows no sawtooth cycle.

for plasma with toroidal magnetic field $B_T = 2.5$ T, radiofrequency (RF)-driven current $I_p = 400$ kA, line-averaged density $\bar{n}_e \sim 3 \times 10^{19} \text{ m}^{-3}$, core electron temperature $T_e \sim 3$ keV, and $\beta_N \sim 1.5$ [$\beta_N = \beta_T / (I_p / a B_T)$], where a is the plasma minor radius, and β_T is defined as the plasma pressure normalized by toroidal magnetic pressure. Plasmas are produced and sustained by RF sources, including lower hybrid wave (LHW) electron cyclotron resonant heating (ECRH) and ion cyclotron resonant heating (ICRH), and neutral beam injection (NBI) heating. RF power remains unchanged after 2.2 s, and two co- I_p neutral beams were turned on in succession after 2.5 s, while a third counter- I_p beam is activated at 3.5 s, as shown in Fig. 1(c). The external loop field E_{loop} drops to almost zero [Fig. 1(d)], indicating the plasma current is driven noninductively. Sawtooth events are not observed, as shown in Fig. 1(e), where only a (1,1) resonant mode appears from 2.5 to 4.5 s [see Fig. 1(e)]. Equilibrium plasma profiles at $t = 3$ s are shown in Fig. 2 [34]. The T_e profile shows a steep gradient near normalized minor radius $r/a \sim 0.19$, while the n_e profile remains relatively flat [see Fig. 2(a) and 2(b)]. The current density profile is monotonically decreasing toward the edge [Fig. 2(c)] and sustained longer than the resistive diffusion time of 1 to 2 s. A relatively flat q profile close to unity in the core area [Fig. 2(d)], and sawtooth-free discharges with active (1,1) mode, are often observed on EAST, suggesting that fluctuation-induced current transport may be occurring to prevent further current profile peaking and sawteeth [15].

In order to determine the fluctuation-induced dynamo, the correlations of magnetic fluctuation with electron temperature

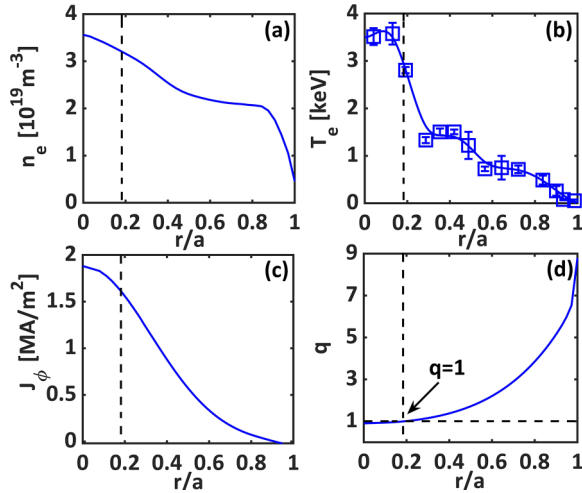


FIG. 2. Profile of (a) electron density, (b) electron temperature showing a steep gradient near $r/a \sim 0.19$, (c) total current density driven by rf and NBI power with no inductive loop voltage, and (d) safety factor q —flat and close to unity for $r/a < 0.19$. Profiles are at $t = 3$ s, and the inverted profile of unity is estimated to be $\sim 15\%$. The vertical black dashed lines indicates the $q = 1$ surface.

fluctuation and density fluctuation are measured using a high-speed ($1\mu\text{s}$), Faraday-effect polarimeter-interferometer system (POINT) [35] with 11 horizontally viewing chords (separation, 8.5 cm). The line-integrated density and Faraday rotation are $\phi_I = 2.82 \times 10^{-15} \lambda \int n_e(R, Z) dR$ and $\Psi_F = 2.62 \times 10^{-13} \lambda^2 \int n_e(R, Z) B_R(R, Z) dR$, respectively, where dR is the plasma path length along the major radius, $B_R(T)$ is the magnetic field component in the radial direction (parallel to the viewing line), and (R, Z) are the radial and vertical positions in the tokamak coordinate system, respectively. The first-order perturbation for interferometry and polarimetry can be expressed as $\delta\phi_I \sim \int \delta n_e dR$, $\delta\Psi_F \sim \int n_e \delta B_R dR$ [13], respectively, where $\int \delta n_e B_R dR$ for viewing lines at or near the magnetic axis can be neglected [36].

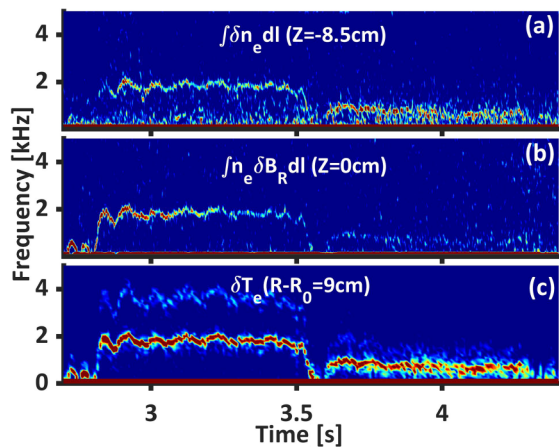


FIG. 3. Spectrogram of (a) density fluctuations at $Z = -8.5$ cm, (b) radial magnetic fluctuation at $Z = 0$, and (c) electron temperature fluctuation near the $q = 1$ resonant surface.

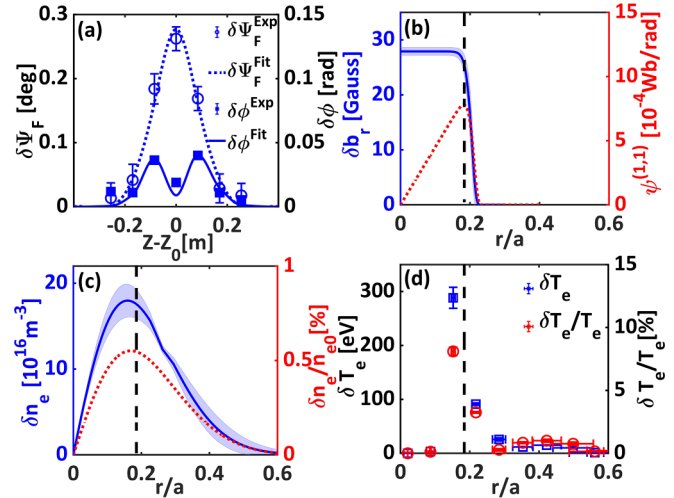


FIG. 4. For the (1,1) kink mode at $t = 3$ s, (a) Faraday fluctuation (circles) profile with the best fit from inversion (dotted line), and interferometer density fluctuation (squares) with the best fit from inversion (solid line), (b) δb_r profile (blue solid line with shaded error) and corresponding $\psi^{1,1}$ profile (red dotted line), (c) δn_e profile (blue solid line with shaded error) and $\delta n_e/n_e$ (red dotted line), and (d) δT_e profile (blue squares) and $\delta T_e/T_e$ (red circles). The vertical black dashed lines indicate the $q = 1$ resonant surface.

Spectrograms of the density $\int \delta n_e dR$ [Fig. 3(a)], radial magnetic $\delta B_R \sim \int n_e \delta B_R dR$ [Fig. 3(b)], and local electron temperature fluctuations [Fig. 3(c)] near $q = 1$ resonant surface (r_s) exhibit a low-frequency ($f \sim 2$ kHz) oscillation, which arises from a (1,1) kink/tearing mode rotating with plasma velocity (V_0) in a laboratory frame. The frequency can vary during the discharge due to velocity change induced by NBI ($\omega = \vec{k} \cdot \vec{V}_0$, where k is the mode wave number); therefore, fluctuation amplitude in the frequency domain corresponds to the amplitude in the space domain. This mode has a strong core-localized magnetic fluctuation with an amplitude that tends to decrease when β_N gradually ramps up. This implies the mode is more kink-like and driven by the current gradient.

To determine the diamagnetic dynamo effect experimentally, one requires the local amplitude of radial magnetic fluctuations perpendicular to magnetic flux surfaces, δb_r . Faraday-effect polarimetry can provide a measure of the line-integrated radial magnetic fluctuation in the high-temperature plasma core [36–38]. The measured Faraday-effect fluctuation amplitude at different impact parameters Z is shown as open circles in Fig. 4(a), at $t = 3$ s using time averaged over 100 ms. The Faraday-effect (magnetic) perturbation peaks at the magnetic axis, as expected for an $m = 1$ current perturbation near the resonant surface. The density perturbations [solid squares in Fig. 4(a)] have a minimum at the magnetic axis and reach a maximum near the resonant surface, as expected for a (1,1) density perturbation.

In order to obtain the local δb_r profile, a reconstruction method based on Newcomb's equation is used [39]. The perturbed flux eigenfunction is assumed to have form $\psi^{1,1}(r) = \psi_0 \times r^\kappa \times e^{-(r/r_s)^\gamma}$ and $\delta \vec{b} = -\nabla \psi^{1,1} \times \hat{\phi}$, where $\hat{\phi}$ indicates the toroidal direction, $\delta B_R = \delta b_r \cos\theta - \delta b_\theta \sin\theta$,

and $\nabla \cdot \delta \vec{b} = 0$ is satisfied [40]. The free parameters ψ_0 , κ , r_s , and γ are adjusted to minimize the difference between the calculated line-integrated fluctuation based on assumed eigenfunction and the experimental data from the density-weighted Faraday-effect fluctuation measurement. The dotted line in Fig. 4(a) is the calculated Faraday-effect fluctuation from fitting experimental data (open circles), where the error bars result primarily from statistical noise. The corresponding eigenfunction profile, $\psi^{1,1}$, can be obtained as shown by the red dotted line [Fig. 4(b)], where the perturbed flux dominates inside the resonant surface. Therefore, the radial magnetic perturbation profile can be determined directly by $\delta b_r = -i\psi^{1,1}/r$, shown by blue solid line [Fig. 4(b)]. The δb_r amplitude ($\delta b_r \sim 30$ Gs; $\frac{\delta b_r}{B_r} = 1.2 \times 10^{-3}$) remains nearly constant inside the resonant surface and falls off quickly toward the wall.

The local amplitude of δn_e for (1,1) mode [see Fig. 4(c)] is achieved by inverting the line-integrated value $\int \delta n_e dR$ measured by interferometry [squares in Fig. 4(a)]. By minimizing the difference between the experimental data [shown as solid squares in Fig. 4(a)] and the calculated line-integrated fluctuations based on the function $\delta n_e^{1,1}(r) = \delta n_{e0} \times r^\kappa \times e^{-r/r_s}$ [shown as a solid line in Fig. 4(a)], one can determine the free parameters (δn_{e0} , r_s , κ , and γ) to obtain $\delta n_e(r)$. The density fluctuation has a maximum near the resonant surface and falls rapidly toward the magnetic axis, where the density gradient is zero, and the plasma edge, where $\delta b_r \sim 0$. The relative density fluctuations have maximum $\delta n_e/n_e \sim 0.5\%$, with a similar profile shape to the density fluctuations [see Fig. 4(c)].

Electron temperature fluctuations are locally measured by a 32-channel heterodyne electron cyclotron emission (ECE) radiometer viewing radially along the midplane [41]. The relative electron temperature fluctuation amplitude, $\delta T_e/T_e$, is obtained directly from the ECE signals. Furthermore, the absolute electron temperature fluctuation amplitude, δT_e , is obtained by combining ECE and Thomson scattering (TS) measurements [Fig. 2(b)]. As shown in Fig. 4(d), maximum $\delta T_e \sim 300$ eV inside the (1,1) resonant surface. $\delta T_e/T_e \sim 10\%$ is much greater than $\delta n_e/n_e \sim 0.5\%$, which is also consistent with the strong harmonic oscillations for δT_e seen in Fig. 3(c). Therefore, the diamagnetic dynamo effect resulting from δT_e is expected to dominate. Both electron temperature and density fluctuations driven by magnetic perturbations most likely arise from field line advection [42].

To evaluate the dynamo emf, the correlated product of δT_e and δb_r can be obtained by ensemble averaging. In EAST, toroidal rotation of the low n magnetic modes transfers their spatial structure in the plasma frame into a temporal evolution in the laboratory frame. Therefore, the mean correlated product of electron temperature and radial magnetic field fluctuations $\langle \delta T_e \delta b_r \rangle = \gamma |\delta T_e| |\delta b_r| \cos \delta \phi_{Tb}$ is evaluated by ensemble averaging over a number of realizations in the 3- to 3.4-s time window, where γ and $\delta \phi_{Tb}$ are the coherence and phase difference between δT_e and δb_r , respectively. A toroidal separation of $\pi/8$ between the two measurements has been corrected to determine $\delta \phi_{Tb}$ for the ensemble average. Technically, δT_e signals are phase-shifted by $\pi/8$ in the frequency domain using Hilbert transformation before performing the ensemble average. In this way, two measurements (δb_r , δT_e) are effectively considered at the same toroidal location.

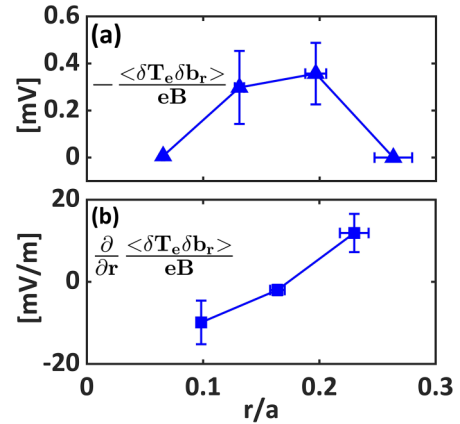


FIG. 5. Profiles of (a) the mean correlated product $-\frac{\langle \delta T_e \delta b_r \rangle}{eB}$ and (b) the temperature fluctuation-driven diamagnetic dynamo $\frac{\partial}{\partial r} \frac{\langle \delta T_e \delta b_r \rangle}{eB}$.

The density fluctuation amplitude ($\sim 0.5\%$) is much smaller than δT_e (about 10%) and negligible, so only the correlated product $-\langle \delta P_e \delta b_r \rangle / e n_e B$ associated with δT_e is shown in Fig. 5(a).

The correlated product $\langle \delta T_e \delta b_r \rangle$ has a maximum value of 0.4 mV inside the resonant surface. For an ideal incompressible linear mode, the phase difference between δT_e and δb_r is $\pi/2$, resulting in a zero correlated product. However, the measured $\langle \delta T_e \delta b_r \rangle$ is nonvanishing experimentally, with δT_e and δb_r being significant, as shown earlier in Fig. 4(b) and 4(d), respectively. Finite $\langle \delta T_e \delta b_r \rangle$ implies the phase difference between the fluctuating parameters slightly deviates from $\pi/2$, and is likely related to turbulence [24]. The experimentally measured fluctuation-induced dynamo profile is shown in Fig. 5(b), determined by calculating the gradient of the electron momentum flux transport. The dynamo is -10 mV/m inside the resonant surface and reverses sign when going across r_s , reaching a maximum of 12 mV/m. The sign change arises from the fact that the correlated product, shown in Fig. 5(a), has a maximum near the resonant surface, causing the gradient of the correlated product to change sign [Fig. 5(a)]. The measured fluctuation-induced dynamo tends to reduce the total current inside the resonant surface and acts to drive the current outside. Hence, the fluctuation-induced dynamo electromotive force tends to transport current away from the plasma core toward the edge, similar to so-called “flux pumping,” thereby preventing current peaking near the magnetic axis.

A (1,1) mode with no sawtooth reconnection during “hybrid” operation has previously been observed in many toroidal magnetic confinement devices [18,19], where the mode was speculated to sustain $q_0 \geq 1$, ($q_0 \cong 2B_T / \mu_0 J_0 R_0$). Our results suggest current density J_0 at magnetic axis is clamped at a level preventing magnetic reconnection (sawtooth crash) by the diamagnetic dynamo effect. To understand the role of a fluctuation-induced dynamo in the current balance in EAST, Eq. (2) can be rewritten as $\eta_{\parallel} (J_{\text{total}} - J_{\text{RF}} - J_{\text{NB}} - J_{\text{BS}}) - E_{\text{ind}} = \text{emf}$, where E_{ind} is the applied inductive field and J_{total} represents the total current density, including the rf wave-driven current J_{RF} , the NBI current J_{NB} , and the bootstrap current J_{BS} [21]. For effective charge $Z_{\text{eff}} \approx 4$ [43] and $\eta_{\parallel} \approx$

2×10^{-8} ohm \cdot m at $r/a = 0.1$, the change of current density by the measured dynamo inside the resonant surface could be -0.5 MA/m². This could reduce the core current by 20% and prevent q_0 from falling to <1 , thereby suppressing the sawtooth instability and magnetic reconnection. Hence, the equilibrium current in EAST is not only determined by an external current drive, but also by the self-generated current (dynamo effect) arising from internal instabilities.

In summary, the first direct fluctuation-induced dynamo measurement has been made in the core of high-

temperature EAST tokamak plasmas. It is found that global MHD instabilities drive a diamagnetic dynamo emf that can serve to transport core parallel current. The diamagnetic fluctuation-induced dynamo provides new insight into current transport in magnetically confined plasmas.

This work was supported by NSFC (Grants No. 11975231 and No. 12127809), and the US DOE (DE-FG03-01ER54615 and DE-FC02-04ER54698).

-
- [1] A. V. Gruzinov and P. H. Diamond, Self-Consistent Theory of Mean-Field Electrodynamics, *Phys. Rev. Lett.* **72**, 1651 (1994).
- [2] I. Gruzinov, A. Das, P. H. Diamond, and A. Smolyakov, Fast zonal field dynamo in collisionless kinetic Alfvén wave turbulence, *Phys. Lett. A* **302**, 119 (2002).
- [3] A. Brandenburg and K. Subramanian, Astrophysical magnetic fields and nonlinear dynamo theory, *Phys. Rep.* **417**, 1 (2005).
- [4] R. H. Levine, Evidence for opposed currents in active region loops, *Sol. Phys.* **46**, 159 (1976).
- [5] S. A. Colgate, T. K. Fowler, H. Li, and J. Pino, Quasi-static model of collimated jets and radio lobes: I. Accretion disk and jets, *Astrophys. J.* **789**, 144 (2014).
- [6] S. A. Colgate, T. K. Fowler, H. Li, E. B. Hooper, J. McClenaghan, and Z. Lin, Quasi-static model of magnetically collimated jets and radio lobes: II. Jet structure and stability, *Astrophys. J.* **813**, 136 (2015).
- [7] E. J. Caramana and D. A. Baker, The dynamo effect in sustained reversed-field pinch discharges, *Nucl. Fusion* **24**, 423 (1984).
- [8] Y.-S. Na *et al.*, Observation of a new type of self-generated current in magnetized plasmas, *Nat. Commun.* **13**, 6477 (2022).
- [9] H. Ji, A. F. Almagri, S. C. Prager, and J. S. Sarff, Time-Resolved Observation of Discrete and Continuous Magnetohydrodynamic Dynamo in the Reversed-Field Pinch Edge, *Phys. Rev. Lett.* **73**, 668 (1994).
- [10] P. W. Fontana, D. J. Den Hartog, G. Fiksel, and S. C. Prager, Spectroscopic Observation of Fluctuation-Induced Dynamo in the Edge of the Reversed-Field Pinch, *Phys. Rev. Lett.* **85**, 566 (2000).
- [11] S. C. Prager, Dynamo and anomalous transport in the reversed field pinch, *Plasma Phys. Controlled Fusion* **41**, A129 (1999).
- [12] D. L. Brower, W. X. Ding, S. D. Terry, J. K. Anderson, T. M. Biewer, B. E. Chapman, D. Craig, C. B. Forest, S. C. Prager, and J. S. Sarff, Measurement of the Current-Density Profile and Plasma Dynamics in the Reversed-Field Pinch, *Phys. Rev. Lett.* **88**, 185005 (2002).
- [13] W. X. Ding, D. L. Brower, D. Craig, B. H. Deng, G. Fiksel, V. Mirnov, S. C. Prager, J. S. Sarff, and V. Svidzinski, Measurement of the Hall Dynamo Effect During Magnetic Reconnection in a High-Temperature Plasma, *Phys. Rev. Lett.* **93**, 045002 (2004).
- [14] H. Ji, Y. Yagi, K. Hattori, A. F. Almagri, S. C. Prager, Y. Hirano, J. S. Sarff, T. Shimada, Y. Maejima, and K. Hayase, Effect of Collisionality and Diamagnetism on the Plasma Dynamo, *Phys. Rev. Lett.* **75**, 1086 (1995).
- [15] S. von Goeler, W. Stodiek, and N. Sauthoff, Studies of Internal Disruptions and $m = 1$ Oscillations in Tokamak Discharges with Soft X-Ray Techniques, *Phys. Rev. Lett.* **33**, 1201 (1974).
- [16] I. T. Chapman, Controlling sawtooth oscillations in tokamak plasmas, *Plasma Phys. Controlled Fusion* **53**, 013001 (2011).
- [17] F. Porcelli, D. Boucher, and M. N. Rosenbluth, Model for the sawtooth period and amplitude, *Plasma Phys. Controlled Fusion* **38**, 2163 (1996).
- [18] J. E. Menard, R. E. Bell, D. A. Gates, S. M. Kaye, B. P. LeBlanc, F. M. Levinton, S. S. Medley, S. A. Sabbagh, D. Stutman, K. Tritz, and H. Yuh, Observation of Instability-Induced Current Redistribution in a Spherical-Torus Plasma, *Phys. Rev. Lett.* **97**, 095002 (2006).
- [19] I. T. Chapman, M.-D. Hua, S. D. Pinches, R. J. Akers, A. R. Field, J. P. Graves, R. J. Hastie, C. A. Michael, and the M. A. S. T. Team, Saturated ideal modes in advanced tokamak regimes in MAST, *Nucl. Fusion* **50**, 045007 (2010).
- [20] Y. Yuan and A. Bhattacharjee, Neoclassical tearing dynamo and self-sustainment of a bootstrapped tokamak, *Phys. Fluids B* **5**, 3661 (1993).
- [21] F. L. Hinton, R. E. Waltz, and J. Candy, Effects of electromagnetic turbulence in the neoclassical Ohm's law, *Phys. Plasmas* **11**, 2433 (2004).
- [22] C. C. Petty, M. E. Austin, C. T. Holcomb, R. J. Jayakumar, R. J. La Haye, T. C. Luce, M. A. Makowski, P. A. Politzer, and M. R. Wade, Magnetic-Flux Pumping in High-Performance, Stationary Plasmas with Tearing Modes, *Phys. Rev. Lett.* **102**, 045005 (2009).
- [23] T. Bando, T. Wakatsuki, M. Honda, A. Isayama, K. Shinohara, S. Inoue, M. Yoshida, G. Matsunaga, M. Takechi, N. Oyama, and S. Ide, Effect of $m/n = 2/1$ neoclassical tearing mode on sawtooth collapse in JT-60U, *Plasma Phys. Controlled Fusion* **63**, 085009 (2021).
- [24] E. Li *et al.*, Experimental Evidence of Intrinsic Current Generation by Turbulence in Stationary Tokamak Plasmas, *Phys. Rev. Lett.* **128**, 085003 (2022).
- [25] P. Piovesan *et al.*, Role of a continuous MHD dynamo in the formation of 3D equilibria in fusion plasmas, *Nucl. Fusion* **57**, 076014 (2017).
- [26] S. C. Jardin, I. Krebs, and N. Ferraro, A new explanation of the sawtooth phenomena in tokamaks, *Phys. Plasmas* **27**, 032509 (2020).
- [27] S. C. Jardin, N. Ferraro, and I. Krebs, Self-Organized Stationary States of Tokamaks, *Phys. Rev. Lett.* **115**, 215001 (2015).

- [28] I. Krebs, S. C. Jardin, S. Günter, K. Lackner, M. Hoelzl, E. Strumberger, and N. Ferraro, Magnetic flux pumping in 3D nonlinear magnetohydrodynamic simulations, *Phys. Plasmas* **24**, 102511 (2017).
- [29] W. X. Wang, T. S. Hahm, E. A. Startsev, S. Ethier, J. Chen, M. G. Yoo, and C. H. Ma, Self-driven current generation in turbulent fusion plasmas, *Nucl. Fusion* **59**, 084002 (2019).
- [30] L. Spitzer, *Physics of Fully Ionized Gases* (Interscience Publishers, New York, 1962), p. 28.
- [31] R. H. Weening and A. H. Boozer, Completely bootstrapped tokamak, *Phys. Fluids B* **4**, 159 (1992).
- [32] H. Ji, S. C. Prager, A. F. Almagri, J. S. Sarff, Y. Yagi, Y. Hirano, K. Hattori, and H. Toyama, Measurement of the dynamo effect in a plasma, *Phys. Plasmas* **3**, 1935 (1996).
- [33] A. M. Garofalo *et al.*, Joint DIII-D/EAST research on the development of a high poloidal beta scenario for the steady state missions of ITER and CFETR, *Plasma Phys. Controlled Fusion* **60**, 014043 (2017).
- [34] J. P. Qian, L. L. Lao, H. Q. Liu, W. X. Ding, L. Zeng, Z. P. Luo, Q. L. Ren, Y. Huang, J. Huang, D. L. Brower, K. Hanada, D. L. Chen, Y. W. Sun, B. Shen, X. Z. Gong, B. J. Xiao, and B. N. Wan, EAST equilibrium current profile reconstruction using polarimeter-interferometer internal measurement constraints, *Nucl. Fusion* **57**, 036008 (2016).
- [35] H. Q. Liu, Y. X. Jie, W. X. Ding, D. L. Brower, Z. Y. Zou, Z. X. Wang, Y. Yang, J. P. Qian, L. Zeng, X. C. Wei, J. S. Shen, Z. H. An, T. Lan, and H. B. Wang, Design of far-infrared polarimeter/interferometer system for EAST tokamak, *J. Instrum.* **8**, C11002 (2013).
- [36] W. X. Ding, D. L. Brower, S. D. Terry, D. Craig, S. C. Prager, J. S. Sarff, and J. C. Wright, Measurement of Internal Magnetic Field Fluctuations in a Reversed-Field Pinch by Faraday Rotation, *Phys. Rev. Lett.* **90**, 035002 (2003).
- [37] J. Chen, D. L. Brower, W. X. Ding, Z. Yan, M. Curie, M. Kotschenreuther, T. Osborne, E. Strait, D. R. Hatch, M. R. Halfmoon, S. M. Mahajan, and X. Jian, Pedestal magnetic turbulence measurements in ELMy H-mode DIII-D plasmas by Faraday-effect polarimetry, *Phys. Plasmas* **28**, 022506 (2021).
- [38] J. Chen, W. X. Ding, D. L. Brower, D. Finkenthal, C. Muscatello, D. Taussig, and R. Boivin, Faraday-effect polarimeter diagnostic for internal magnetic field fluctuation measurements in DIII-D, *Rev. Sci. Instrum.* **87**, 11E108 (2016).
- [39] R. Fitzpatrick, S. C. Guo, D. J. Den Hartog, and C. C. Hegna, Effect of a resistive vacuum vessel on dynamo mode rotation in reversed field pinches, *Phys. Plasmas* **6**, 3878 (1999).
- [40] F. Salzedas, F. C. Schüller, and A. A. M. Oomens, and the RTP team, Exponentially Growing Tearing Modes in Rijnhuizen Tokamak Project Plasmas, *Phys. Rev. Lett.* **88**, 075002 (2002).
- [41] X. Han, X. Liu, Y. Liu, C. W. Domier, N. C. Luhmann, E. Z. Li, L. Q. Hu, and X. Gao, Design and characterization of a 32-channel heterodyne radiometer for electron cyclotron emission measurements on experimental advanced superconducting tokamak, *Rev. Sci. Instrum.* **85**, 073506 (2014).
- [42] M. A. Van Zeeland, G. J. Kramer, M. E. Austin, R. L. Boivin, W. W. Heidbrink, M. A. Makowski, G. R. Mckee, R. Nazikian, W. M. Solomon, and G. Wang, Radial Structure of Alfvén Eigenmodes in the DIII-D Tokamak Through Electron-Cyclotron-Emission Measurements, *Phys. Rev. Lett.* **97**, 135001 (2006).
- [43] Y. Chen, Z. Wu, W. Gao, L. Zhang, and W. Zha, Z_{eff} first measurements in EAST with a multi-channel visible bremsstrahlung new system, *Fusion Eng. Des.* **88**, 2825 (2013).

Correction: During the proof process, centered dots were erroneously changed to multiplication signs in Eq. (3) and in inline equations in the second sentence of both the seventh and ninth paragraphs and have been fixed. Minus signs were missing from exponents in the second sentence of the sixth paragraph and have been inserted.